Journal of Magnetic Resonance **147,** 95–103 (2000)
doi:10.1006/jmre.2000.2185, available online at http://www.idealibrary.com on IDEAL®

Relaxation of Nuclear Magnetization in a Nonuniform Magnetic Field Gradient and in a Restricted Geometry

Lukasz J. Zielinski*,† and Pabitra N. Sen*

**Schlumberger-Doll Research, Old Quarry Road, Ridgefield, Connecticut 06877-4108; and*
†Department of Physics, Harvard University, Cambridge, Massachusetts 02138

Received March 20, 2000; revised August 2, 2000

We study the influence of restriction on Carr–Purcell–Meiboom–Gill spin echo response of magnetization of spins diffusing in a bounded region in the presence of a nonuniform magnetic field gradient. We consider two fields in detail—a parabolic field which, like the uniform-gradient field, scales with the system size, and a cosine field which remains bounded. Corresponding to three main length scales, the pore size, L_S, the dephasing length, L_G, and the diffusion length during half-echo time, L_D, we identify three main regimes of decay of the total magnetization: motionally averaged, localization, and short-time. In the short-time regime ($L_D \ll L_S$, L_G), we confirm that the leading order behavior is controlled by the average of the square of the gradient, $\overline{(\nabla B_z)^2}$, and in the motionally averaged regime (MAv), where $L_S \ll L_D$, L_G, by $\overline{(\int dx B_z)^2}$. We verify numerically that two different fields for which those two averages are identical result in very similar decay profiles not only in the limits of short and long times but also in the intermediate times, with important practical implications. In the motionally averaged regime we found that previous estimates of the decay exponent for the parabolic field, based on a soft-boundary condition, are significantly altered in the presence of a more realistic, hard wall. We find the scaling of the decay exponent in the MAv regime with pore size to be L_S^2 for the cosine field and L_S^6 for the parabolic field, as contrasted with the linear gradient scaling of L_S^4. In the localization regime, for both the cosine and the parabolic fields, the decay exponent depends on a fractional power of the gradient, implying a breakdown of the second cumulant or the Gaussian phase approximation. We also examined the validity of time-evolving the total magnetization according to a distribution of effective local gradients and found that such approximation works well only in the short-time regime and breaks down strongly for long times. © 2000 Academic Press

Key Words: **susceptibility contrast; restricted diffusion; NMR microscopy; confinement; inhomogeneous fields.**

1. INTRODUCTION

The purpose of this paper is to carry on our previous study (*1*) of the relaxation of the Carr–Purcell–Meiboom–Gill (CPMG) spin echo amplitude resulting from the combined effects of diffusion and restricted geometries to the cases of nonuniform gradients. We extend the work of Tarczon and Halperin (*2*) who computed the response for one echo (the Hahn echo) in an arbitrary inhomogeneous field in the Gaussian phase approximation (GPA) to the case of multiple CPMG spin echoes (*3*–*5*). The GPA, or the second cumulant, treatment has been commonly used in the literature (*1*–*4*, *6*, *7*, *10*). In the study of systems with nonuniform magnetic fields, a fruitful approach has been to employ eigenfunction expansion in the basis of the system in the absence of the field (*1*, *7*–*10*). These results, long known for the Hahn echo, have been recently generalized for the CPMG (*10*, *11*).

Although the material presented here partially overlaps with the work of Bergmann and Dunn (*10*) and Brown and Fantazinni (*11*), our emphasis is different in that we consider some simple field profiles in detail to understand the scaling of relaxation rate with pore size. We also consider the behavior in the "localization regime," where the GPA breaks down.

NMR response in a constant gradient has been studied quite extensively since most standard techniques for both diffusion measurements (*3*, *4*, *12*) and NMRI (*12*) involve the application of a constant gradient field. Recent years, however, have seen the emergence of new methods employing strongly inhomogeneous fields for magnetic resonance microscopy, most notably the stray-field imaging (*13*), which is now widely used in the study of diffusion in soil and concrete as well as of the ingress of solvents into polymers. Large inhomogeneities are also generated in bore-hole tools used in geophysical applications (*14*, *15*).

Even when the applied fields are homogeneous, the difference in susceptibility of the constituent materials gives rise to a microscopically inhomogeneous field (*11*, *16*). For example, the susceptibility contrast between pore space and grains in rocks or between tissue and fluid in biological samples (*17*) poses serious problems in NMR imaging and relaxometry. The effects of these microscopic field inhomogeneities cannot always be removed by appropriate pulse sequences. In fact, in many cases they are exploited to diagnose abnormal tissues (*18*). In this light, it is clear that the study of diffusion in arbitrary inhomogeneous fields is important for the understanding of a host of current applications.

The two simple field models we consider in this paper are the natural first step beyond the uniform gradient case: the parabolic field (i.e., the gradient varies linearly) and the cosine field, which has the form identical to the first eigen mode of the

1090-7807/00 $35.00

Fourier expansion of the magnetic field in a simple one-dimensional geometry. The choice of the cosine form was also motivated in part by the fact that the resulting eigenvalue problem bears some resemblance to the constant gradient case (*19*) and that the field is bounded. Accordingly, it captures one characteristic of the microscopic local fields, arising from the susceptibility differences within the grain, which are in general proportional to the applied field and result in a bounded total field. The effects of bounded and unbounded fields differ dramatically in physical systems as shown by Song *et al.* (*20*). In addition, the cosine field provides a simple example of a field where the gradient at the walls vanishes, serving as an unambiguous test of the prediction for the lowest order correction due to restriction to the short-time decay (*1, 10*).

Now let us give a brief outline of the paper. In Section 2 we give the general analytical framework for the solution of the Torrey–Bloch equation and briefly recapitulate the various asymptotic regimes for the CPMG and the numerical procedure employed. In Section 3 we discuss certain results for the transition region between the short-time and motionally averaged regimes. In Sections 4 and 5, we present the numerical and analytical results for the parabolic and cosine fields, respectively. In Section 6, we investigate the applicability of the local gradient approximation (LGA) in the case of our two fields, and we conclude in Section 7.

2. THEORY

2.1. Torrey Equation and the Boundary Condition

We begin with a steady-state magnetization aligned with the applied magnetic field in the z-direction. Following a $\pi/2$ pulse, the transverse magnetization, $M(x, t) = M_x(x, t) + iM_y(x, t)$, obeys Bloch's equation, as modified by Torrey (*21*) to include diffusion,

$$\frac{\partial M(x, t)}{\partial t} = D_0 \frac{\partial^2 M(x, t)}{\partial x^2} - i\gamma B_z(x) M(x, t), \qquad [1]$$

with the initial condition $M(x, 0) = \text{const}$. A factor of $\exp(-i\omega_0 - 1/T_{2B})t$ has been divided out of $M(x, t)$, where $\omega_0 = \gamma B_0$ is the average Larmor frequency, T_{2B} is the bulk decay time constant, and D_0 is the diffusion coefficient, which is a function of temperature and pressure. The boundary condition on the pore wall is

$$D_0 \frac{\partial M(x, t)}{\partial \nu} + \rho M(x, t) = 0, \qquad [2]$$

where the operator $\partial/\partial\nu$ is the outgoing (from pore into grain) normal derivative and ρ is the surface relaxativity. In the remainder of the paper we take $\rho = 0$, which is equivalent to imposing the reflecting boundary conditions.

2.2. Relaxation Regimes for Hahn and CPMG Echoes

In this section we give a brief summary of various regimes of decay as previously treated in (*1, 6, 22*). With the surface relaxativity set to zero, the attenuation of spin echoes due to restricted diffusion in a nonuniform gradient field can be characterized by three lengths: the diffusion length, $L_D = \sqrt{D_0\tau}$, the sample size, L_S (we consider only one-dimensional samples), and the dephasing length,

$$L_G = \left[\frac{D_0^2}{\overline{(\nabla B_z)^2}\gamma^2}\right]^{1/6} = \left[\frac{D_0^2}{g^2\gamma^2}\right]^{1/6}, \qquad [3]$$

where D_0 is the diffusion coefficient, τ is half the echo time, and $g^2 \equiv \overline{(\nabla B_z)^2}$ is the mean-squared gradient. The overbar signifies a spatial average. The diffusion length is a measure of the distance traveled by a spin in the time τ. The dephasing length gives the distance over which a spin has to diffuse to dephase by 2π radians.

Corresponding to these three length scales, there are three asymptotic rates of relaxation of the spin echo amplitude (*1*), determined by the shortest length scale. Accordingly, we distinguish three regimes: short-time where $L_D \ll L_S, L_G$; motionally averaged where $L_S \ll L_D, L_G$; and localization where $L_G \ll L_D, L_S$.

The short-time and motionally averaged regimes can be treated within the GPA, whose validity in these regimes can be physically motivated as follows. As noted above, at short times t, only a small fraction of the spins, on the order of $\sqrt{(D_0t)}\, S/V_p$, interacts with the walls, S/V_p being the surface to volume ratio and D_0 the free diffusion coefficient. Accordingly, we expect the GPA to hold. In the motionally averaged regime once a spin traverses a pore several times it loses the memory of where it started. At long times then, the phase accumulation of an individual spin can be represented as a sum of many small independent phase accumulations over a few traversals of the pore. Hence, we may expect that the GPA can be reasonably good at both short and long times outside of the localization regime.

First we consider the GPA and its two limiting cases. The Bloch–Torrey equation is solved exactly within the GPA for the CPMG by Bergman and Dunn in (*10*) (see Eqs. [3.2] and [3.3] therein) following Brown and Fantazzini in (*11*). Here we recast the solution in a slightly different form and correct a typographical error (the same equation is derived by a different method in (*23*):

$$-\ln\left[\frac{M(2n\tau)}{M(0)}\right] = \tilde{\gamma}^2 \sum_{\alpha>0} |\tilde{b}_\alpha|^2 \left[2n\left(\frac{\tilde{D}_0\tilde{\lambda}_\alpha - \tanh(\tilde{D}_0\tilde{\lambda}_\alpha)}{(\tilde{D}_0\tilde{\lambda}_\alpha)^2}\right) + \frac{\tanh^2(\tilde{D}_0\tilde{\lambda}_\alpha) - 2(1 - \operatorname{sech}(\tilde{D}_0\tilde{\lambda}_\alpha))}{(\tilde{D}_0\tilde{\lambda}_\alpha)^2} \times (1 - (-1)^n e^{-2n\tilde{D}_0\tilde{\lambda}_\alpha}) \right], \qquad [4]$$

where $\tilde{b}_\alpha$ are the expansion coefficients of the magnetic field in an eigenbasis, $\tilde{\lambda}_\alpha$ are the corresponding eigenvalues, $\tilde{\gamma} = L_D^2 L_S / L_G^3$ is the dimensionless gyromagnetic ratio, and $\tilde{D}_0 = (L_D/L_S)^2$ is the dimensionless diffusion constant. (See Section 5 for an application of Eq. [4].) For $n = 1$, i.e., the Hahn echo, Tarczon and Halperin (*2*) derive an equivalent of Eq. [4] for one dimension.

The leading term of the short-time limit of Eq. [4] is

$$\frac{M(2n\tau)}{M(0)} = e^{-(2n/3)(L_D/L_G)^6}. \qquad [5]$$

For slightly longer times, but still when few spins make contact with the walls, the lowest order correction to the CPMG-generalized Hahn result, Eq. [5], is proportional to L_D/L_S. It was computed for the Hahn echo in (*6*) and can be obtained for the CPMG from Eq. [4]:

$$\frac{M(2n\tau)}{M(0)} = e^{-(2/3)(L_D/L_G)^6(n + C(n)(L_D/L_S)(g_\nu^2/g^2))}. \qquad [6]$$

Here $C(n)$ is a constant that depends only on the echo number and has been calculated explicitly (*1*), $g^2 = 1/L_S \int dx |\partial B/\partial x|^2$ as before, and

$$g_\nu^2 = \frac{1}{S} \oint_{\partial\Omega} \left(\frac{\partial B_z}{\partial \nu}\right)^2 \qquad [7]$$

is the surface average of the normal derivative of the field, where S is the pore surface area. The physical implication of the appearance of g_ν, which captures the dependence on the geometry of the interface, is that often the presence of paramagnetic impurities near pore boundaries makes the field at the pore wall considerably different from that in the interior.

Next we consider the motionally averaged (long-time) limit of the GPA. Here the spins typically diffuse several times the dimension of the pore, and any magnetic field inhomogeneities are averaged out by their motion. The asymptotic form of the decay exponent was derived for an arbitrary field for the Hahn echo in one-dimensional restricted geometry by Tarczon and Halperin (*2*) and can be obtained for the CPMG from Eq. [4] as

$$-\ln\left[\frac{M(2n\tau)}{M(0)}\right] = 2n\,\frac{L_D^2 L_S^4}{L_G^6} \sum_{\alpha>0} \frac{|\tilde{b}_\alpha|^2}{\tilde{\lambda}_\alpha}$$
$$= \frac{2n\tau\gamma^2}{D_0} \overline{\left(\int_0^x B_z(x')dx'\right)^2}, \qquad [8]$$

where 2τ is the time between successive π pulses and the overbar denotes a spatial average as before. The last part of this equation is valid only in one dimension. The leading-order correction can be computed by taking the long-time limit of Eq. [4].

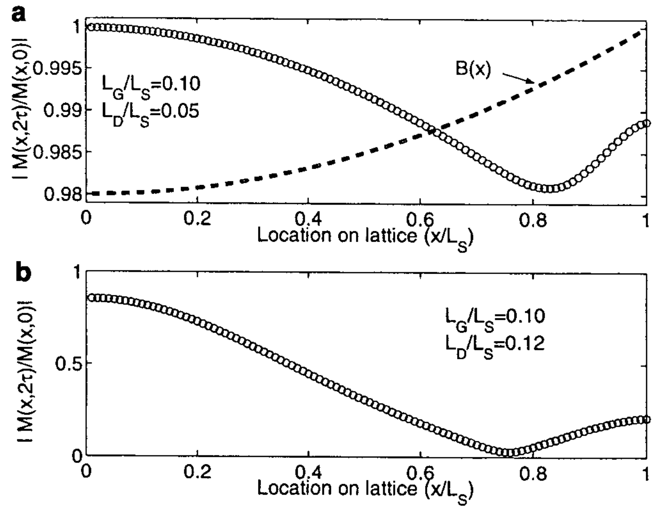

FIG. 1. Position dependence of the transverse magnetization at the first echo in a parabolic magnetic field (profile drawn in dashed lines in arbitrary units) in the localization regime at two different echo times: (a) short ($L_D \ll L_G, L_S$) and (b) longer ($L_D \sim L_G \ll L_S$). The signal accumulates near the walls and near the field minima, decaying fastest in regions of large gradient away from walls.

Finally, we consider the case where the GPA breaks down: the localization regime. Here the spins diffuse several dephasing lengths in the course of a measurement, dephasing by a very large amount. Their net contribution to the total magnetization vanishes, except for those located near the field minima and near the boundaries, which, because of reflection, see a smaller change in the magnetic field and consequently dephase less. Using this approximation, one can try to solve the eigenvalue problem obtained by separating variables in Eq. [1], the long-time decay rate being determined by the lowest eigenvalue in the presence of the magnetic field (*6*, *19*). In other words, the GPA treats the magnetic field inhomogeneity perturbatively, while in the localization regime, it must be treated exactly.

To lend justification to the above qualitative picture of the dependence of the magnetization on the local gradient and distance to the boundaries, we plot in Fig. 1 the transverse magnetization as a function of position at two different times in a parabolic magnetic field with the tip of the parabola at the left wall. Magnetization accumulates near the left-hand wall, where the field minimum coincides with the proximity of the wall. It decays faster with increasing gradient, until the effects of the presence of the right wall counteract the trend, resulting in a pronounced dip in the middle. In Fig. 1b, where the diffusion length, L_D, is on the order of the dephasing length, L_G, the magnetization has decayed virtually to zero near the dip while remaining sizable near both walls.

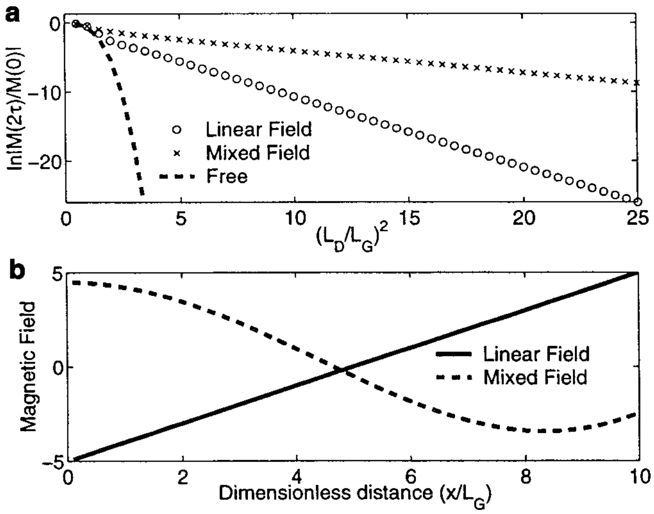

FIG. 2. (a) Localization regime: relative height of the first echo ($n = 1$) in a linear field (open circles) and "mixed" field (labeled by $\times$), with identical averages $\overline{(\partial B_z/\partial x)^2}$ and $\overline{(\int dxB_z)^2}$. Here the precise field landscape, not just the averages, is important, resulting in different decay rates (slopes). The free-diffusion result, Eq. [5], the same for both fields, is drawn as a dashed line for comparison. (b) The two field profiles plotted, in arbitrary units, as a function of position in the pore.

2.3. Numerical Method

The numerical procedure we use to solve the Torrey–Bloch equation is exactly the same as in our previous work (*1*) and is outlined there in detail. We need not repeat the details here.

3. INTERPOLATION BETWEEN REGIMES

Although the long and the short time limits of the solutions of Eq. [1] for different field profiles and boundary conditions have been studied extensively, no tractable analytical expressions exist for the intermediate regimes. In this section we present the results of a numerical experiment that sheds some light on the behavior of $M(2n\tau)$ in the transition region. We constructed two qualitatively different fields with identical averages, $\overline{(\partial B_z/\partial x)^2}$ and $\overline{(\int dxB_z)^2}$, which guarantees the same asymptotic behavior in the short-time and motionally averaged regimes. In particular we took $B_1(x) = C_1\cos(\pi x/L_S) + C_2x^2 - \frac{1}{3}L_S^2C_2$ and $B_2(x) = gx - \frac{1}{2}gL_S$, where $C_1 = 0.6508\ gL_S$ and $C_2 = 0.608\ g/L_S$, chosen to make the corresponding averages for each field equal. Both fields are plotted in Fig. 2b. Figure 2a shows that in the localization regime, where we don't expect Eq. [8] to hold, the decay exponent approaches different values since it is determined by the lowest eigenvalue, which, in turn, depends on the local structure of the field inhomogeneities. This is to be contrasted with the regimes where the GPA holds. In the short-time and motionally averaged regimes, graphed in Figs. 3a and 3b, respectively, magnetization approaches the same limits, as expected. Remarkably, however, the signal for both fields is virtually identical for *all* times. This suggests that the system smoothly "interpolates" between the asymptotic regimes in much the same way regardless of the precise form of the magnetic field present. In other words, the behavior of $M(t)$ outside of the localization regime is governed entirely (in one dimension) by the spatial averages of field-related quantities, not by any other local details of the structure of the field itself.

4. PARABOLIC FIELD

In this section we study the various regimes for the case of the parabolic field, $(B_0 + g_1x + g_2x^2)\hat{\mathbf{z}}$. First consider the effect of the presence of walls. Le Doussal and Sen (*24*) solved exactly the free diffusion Torrey equation for this field. Here we find their analytical results to be in excellent agreement with our computer simulations as long as the walls are far away, i.e., $L_S \gg L_D$, L_G. They also simulated the effect of restriction by imposing a "soft" boundary condition by adding a restoring potential to the diffusion equation and solving it as an unbounded problem. Within this model, in the motionally averaged regime, they found that the decay rate

$$\frac{1}{2n\tau}\ln\left(\frac{M(2n\tau)}{M(0)}\right) \rightarrow \frac{\gamma^2g_2^2L_S^6}{8D_0} \qquad [9]$$

for $g_1 = 0$ in sharp contrast with Eq. [8] which gives

$$\frac{1}{2n\tau}\ln\left(\frac{M(2n\tau)}{M(0)}\right) \rightarrow \frac{8\gamma^2g_2^2L_S^6}{945D_0}, \qquad [10]$$

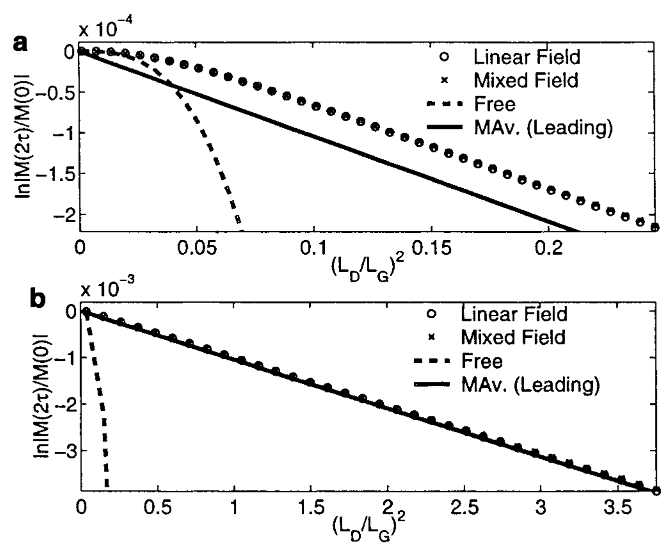

FIG. 3. Relative height of the first echo ($n = 1$) in the two fields shown in Fig. 2b, linear (open circles) and "mixed" (labeled by $\times$), with identical $\overline{(\partial B_z/\partial x)^2}$ and $\overline{(\int dxB_z)^2}$ averages in the short-time regime (a) and the motionally averaged regime (b). The free-diffusion result, Eq. [5], is drawn as a dashed line, and the motionally averaged regime leading asymptotic, Eq. [8], as a solid line. Note that both field profiles result in virtually indistinguishable signals for *all* time.

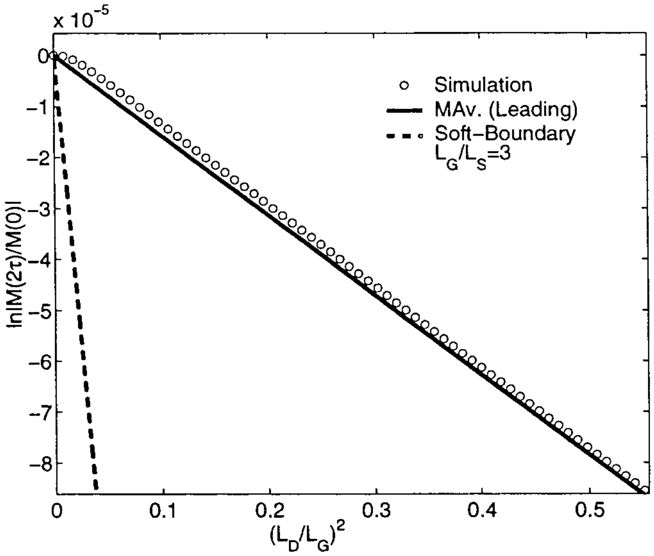

FIG. 4. Motionally averaged regime: relative height of the first echo (n = 1) in a parabolic field. Simulation (open circles) plotted against the predictions of the soft-boundary model, Eq. [9] (dashed line), and the GPA with hard walls in the motionally averaged regime, Eq. [10] (solid line). Note the dramatic failure of the soft-boundary model.

which is about a factor of 15 less than the result of Le Doussal and Sen.

Our numerical simulations (see Fig. 4) confirm the prediction of Eq. [10] demonstrating that the presence of the real wall substantially reduces decay. Although Le Doussal and Sen's decay exponent, Eq. [9], displays the correct pore-size scaling, L_S^6 for the parabola vs L_S^4 for the linear gradient, it fails to give the correct magnitude of the decay rate which is in agreement with Eq. [10], the asymptotic mean-field result based on Eq. [8].

In the localization regime, on the other hand, the soft-boundary model does produce the correct behavior, giving $\sqrt{\frac{1}{2} g_2 \gamma D_0}$ for the decay rate in good accord with our simulations (see Fig. 5).

Now consider the short-time regime and the correction due to pore surface to volume ratio. In the short-time regime, with the walls placed at the origin and at L_S and $g_1 = 0$, we compute $g^2 = \frac{4}{3} g_2^2 L_S^2$ and $g_\nu^2 = 2 g_2^2 L_S^2$, and Eq. [6] gives

$$\ln\left(\frac{M(2n\tau)}{M(0)}\right) = -\frac{2}{3}\left(\frac{L_D}{L_G}\right)^6\left(n + 1.5\ C(n)\left(\frac{L_D}{L_S}\right)\right). \quad [11]$$

Our numerical simulations, as shown in Fig. 6, are in excellent agreement with Eq. [11]. Note the enhancement of the impact of the boundary effects due to the increased curvature of the field at the wall relative to the uniform-gradient case. In that case $g = g_\nu$, and consequently the factor multiplying the first-order correction in L_D/L_S is 1 instead of 1.5. For the cosine

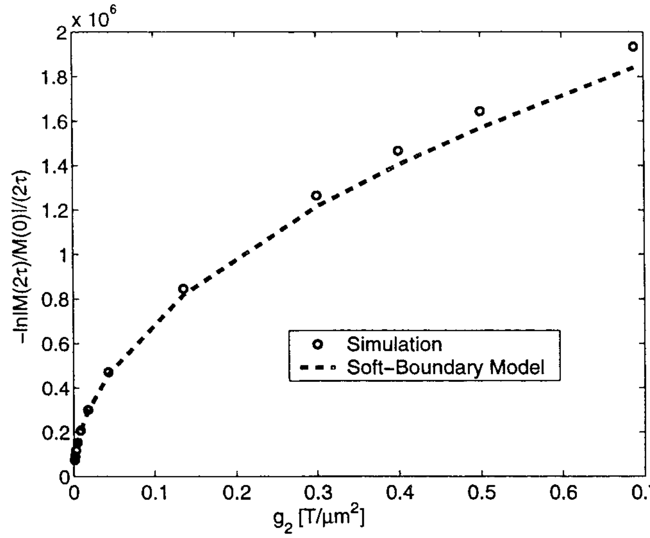

FIG. 5. Localization regime: decay rate of the magnetic density signal at the first echo in the parabolic field $B_z(x) = g_2 x^2$. Simulation results (open circles) are plotted vs the prediction of Le Doussal and Sen's soft-boundary model, Eq. [9] (dashed line). The $\sqrt{g_2}$ dependence indicates the breakdown of the GPA.

field, on the other hand, to be discussed in detail in the next section, the presence of the wall will be less noticeable in the short-time regime due to the vanishing of g_ν and the resulting suppression of the L_D/L_S correction.

5. COSINE FIELD

In this section we study the cosine field, $B_0 \cos(\pi x/L_S)\hat{\mathbf{z}}$. Note that the field is bounded by B_0 which is independent of

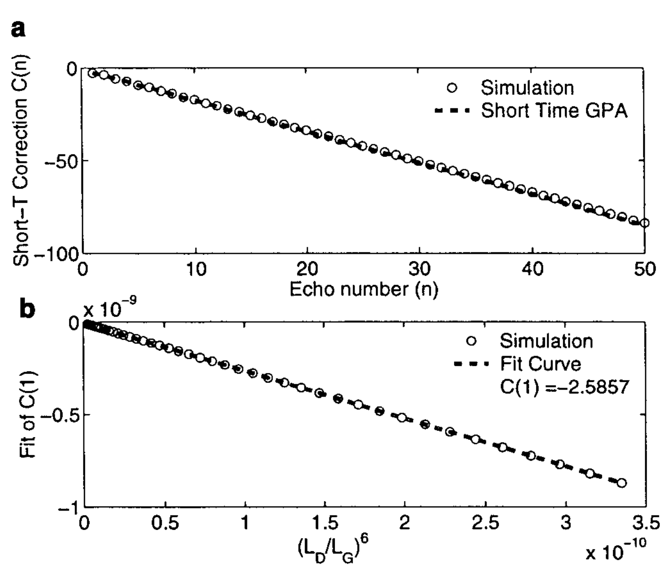

FIG. 6. (a) Short-time linear correction coefficient $C(n)$ for the parabolic field case as a function of the echo number. Simulation results (open circles) plotted vs the GPA theory, Eq. [11] (dashed line). (b) Plot of the actual simulation data for the first echo from which $C(1)$ was extracted.

the system size as opposed to the linear and parabolic fields which grow with L_S. To obtain the equations governing the short-time and motionally averaged regimes, we use Eq. [4]. As the eigenbasis for the expansion in Eq. [4] we take the eigenfunctions of ∇^2 with the reflecting boundary conditions, at $\tilde{x} = 0$ and $\tilde{x} = 1$ in dimensionless coordinates $\tilde{x} \equiv x/L_S$, namely $\Psi_\alpha = N_\alpha \cos(\pi\alpha\tilde{x})$ where $\alpha = 0, 1, 2, \ldots$, and N_α is the normalization constant. Then $\tilde{b}_\alpha \equiv \int_0^1 \tilde{B}(\tilde{x})\Psi_\alpha(\tilde{x})d\tilde{x}$ vanishes for all $\alpha \neq 1$. The sum in Eq. [4] reduces to a single term,

$$-\ln\left[\frac{M(2n\tau)}{M(0)}\right] = \tilde{\gamma}^2\left|\frac{\tilde{b}}{\sqrt{2}}\right|^2\left[2n\left(\frac{\tilde{D}_0\pi^2 - \tanh(\tilde{D}_0\pi^2)}{(\tilde{D}_0\pi^2)^2}\right) + \frac{\tanh^2(\tilde{D}_0\pi^2) - 2(1 - \mathrm{sech}(\tilde{D}_0\pi^2))}{(\tilde{D}_0\pi^2)^2} \times (1 - (-1)^n e^{-2n\tilde{D}_0\pi^2})\right]. \quad [12]$$

The short-time limit of Eq. [12] shows that the linear correction in L_D/L_S vanishes in agreement with Eq. [11], given that $g_\nu = 0$ in one dimension for this particular field profile:

$$-\ln\left(\frac{M(2n\tau)}{M(0)}\right) \overset{\tau\to\infty}{\sim} \frac{2}{3}\left(\frac{L_D}{L_G}\right)^6\left[n - \frac{3}{8}(1 - (-1)^n)\pi^2\left(\frac{L_D}{L_S}\right)^2\right]. \quad [13]$$

We found very good agreement between the analytical expressions in Eqs. [12] and [13] and our simulations for both the short-time and the motionally averaged regimes. Note that in Eq. [13], the leading order correction vanishes for the even echoes and for odd echoes is proportional to $(L_D/L_S)^2$, as opposed to L_D/L_S correction for a field with a constant gradient. On the other hand, for any field with an odd reflexion geometry, e.g., $B_0\sin(\pi x/L_S)$, the leading order correction due to restriction would be identical to that for the constant gradient case. In Fig. 9 we plot the general GPA solution for the cosine field, Eq. [12], vs simulation in the short-time (Fig. 9a), and motionally averaged (Fig. 9b) regimes.

It is instructive to consider the long-time limit of Eq. [12] in order to examine the scaling of the decay rate with the size of the pore:

$$-\ln\left(\frac{M(2n\tau)}{M(0)}\right) \overset{\tau\to\infty}{\sim} \frac{2n}{\pi^4}\left(\frac{L_D}{L_G}\right)^2\left(\frac{L_S}{L_G}\right)^4\left[1 - \frac{2n+1}{2\pi^2 n}\left(\frac{L_S}{L_D}\right)^2\right]. \quad [14]$$

From the definition of dephasing length, Eq. [3], we find for the cosine field

$$L_G^3 = \frac{\sqrt{2}\, D_0 L_S}{\pi B_0 \gamma},$$

which in conjunction with Eq. [14] shows that the long-time exponent $\sim L_S^2$. This indicates that the dependence of the signal decay rate with pore size is markedly less for the cosine field than for either the linear ($\sim L_S^4$) or the parabolic ($\sim L_S^6$) field. From the dependence of the exponent on $\overline{(\int dxB_z)^2}$ we expect this result to hold more generally for the case of bounded vs unbounded fields.

In the localization limit the GPA is not valid. The eigenvalue equation derived from the Torrey–Bloch equation, Eq. [1], for the cosine field in scaled coordinates is the Mathieu equation (*19, 25*):

$$\frac{d^2 m_i}{d\tilde{y}^2} + [\tilde{E}_i - 2q\cos(2\tilde{y})]m_i = 0, \quad [15]$$

where $\tilde{y} = \pi x/2L_S$, $q = i[\sqrt{2}\, L_S/\pi L_G]^3$, $\tilde{E}_i = (4/\pi^2)(L_S/L_G)^2 E_i$. The general solution for the magnetization in terms of the eigenfunctions m_i is

$$M(x, t) = \sum c_i m_i(x) e^{-E_i t}.$$

In the localization regime, $|q| \gg 1$, and we use a large-q expansion for the lowest eigenvalue for real q (*25*), which we verified numerically to hold for large imaginary q as well:

$$\tilde{E}_0 \simeq -2q + 2\sqrt{q}.$$

The rate of decay is then determined by the real part of $\tilde{E}_0 \simeq \sqrt{2|q|}$, and we finally obtain

$$\frac{M(2n\tau)}{M(0)} \propto e^{-(2\pi^2)^{1/4} n (L_G/L_S)^{1/2} (L_D/L_G)^2}. \quad [16]$$

The constant of proportionality depends on the integrals of the eigenfunctions and their normalization constant (*6*). Our simulations for the localization regime confirm the anticipated exponent (see Fig. 7). A noteworthy characteristic of Eq. [16] is that the decay exponent varies as $L_G^{-3/2}$ and hence $\sqrt{B_0}$, indicating the breakdown of the GPA, and varies inversely with $\sqrt{L_S}$, unlike for the case of the linear and parabolic fields for which it is independent of L_S in the localization regime. Dependence of the localization exponent on the pore size may be a general feature of bounded fields. Recall that the bounded fields commonly originate from susceptibility variations within the sample, in contrast to the unbounded fields originating from externally applied gradients.

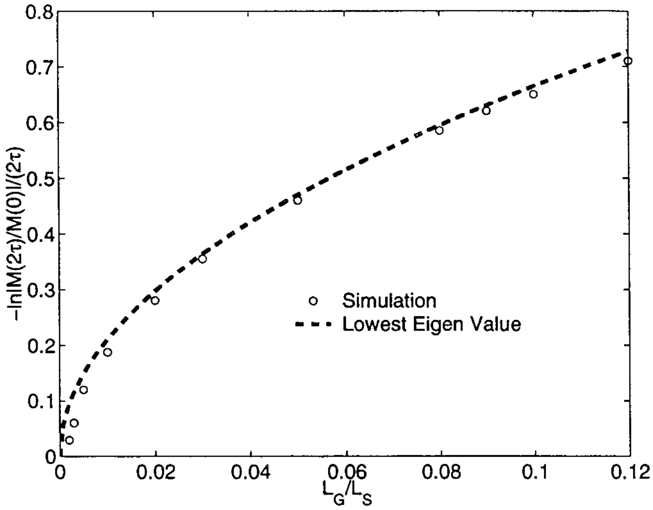

FIG. 7. Decay rate of the first echo for the cosine field in the localization regime as a function of L_G/L_S. Simulation results (open circles) are compared with the lowest eigenmode of the Torrey–Bloch equation as computed in Eq. [16] (dashed line). The $\sqrt{L_G/L_S}$ and hence $\sqrt{B_0}$ dependence implies the breakdown of the GPA.

6. LOCAL GRADIENT APPROXIMATION

It is a common practice (*26, 27*) to invoke an average local gradient in order to capture the effects of the inhomogeneities of the magnetic field. We test the range of validity of this ansatz for the cosine and parabolic fields.

At very short times, it is legitimate to represent an arbitrary field by an effective local gradient, $g_{\mathrm{eff}} = g_1 + 2g_2x + \cdots$. If the diffusion length L_D is small compared to the lengths over which g_{eff} varies, then locally, $M(x)$ obeys the CPMG-generalized Hahn's formula, Eq. [5]. Integrating over the entire sample, we obtain

$$\frac{M(2n\tau)}{M(0)} = \int P(g_{\mathrm{eff}})e^{-2/3\gamma^2 g_{\mathrm{eff}}^2 D_0 n\tau^3} dg_{\mathrm{eff}}, \qquad [17]$$

where $P(g_{\mathrm{eff}})$ is the distribution function of the effective gradients, $P(g) \equiv \int_0^{L_S} dx\,\delta[g - dB(x)/dx]$. Although strictly valid only for the short times, Eq. [17] has been frequently applied over the whole range of time. For the parabolic field, setting $g_1 = 0$ as before, $P(g) = (2g_2L_S)^{-1}$, and Eq. [17] gives

$$\frac{M(t)}{M(0)} = \frac{\sqrt{\pi}}{2\beta}\,\mathrm{erf}(\beta),$$

where $\beta^2 = \frac{2}{3}(L_D/L_G)^6$, and $\mathrm{erf}(\beta)$ is the error function. Note that in the limit of small β this correctly reduces to the leading term of the CPMG short-time formula, Eq. [5]. For the cosine

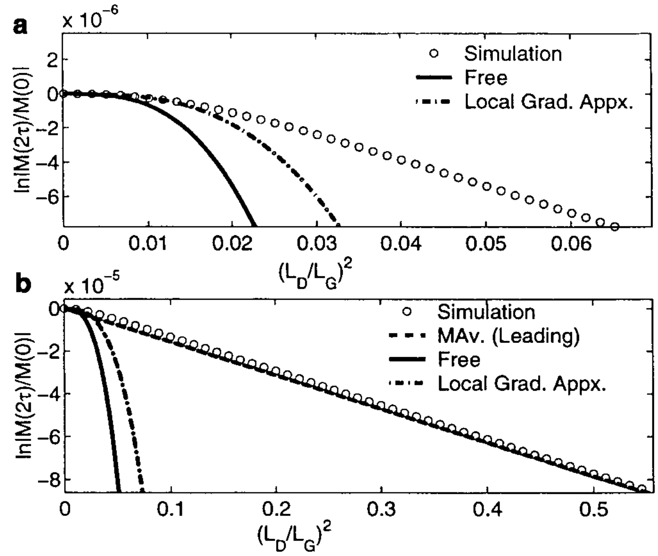

FIG. 8. Comparison of the local gradient approximation (LGA) for the parabolic field (dot–dashed line) with the simulation data (open circles) and the GPA limits (free diffusion in solid and leading order motionally averaged in the dashed line) for the first echo in (a) short-time and (b) motionally averaged regimes. Note that the LGA performs better than the leading term of the short-time GPA limit (free diffusion), Eq. [5], but breaks down strongly in the motionally averaged regime.

field, $P(g) = 2L_S/B_0\pi^2\,[1 - g^2L_S^2/\pi^2B_0^2]^{-1/2}$, and the LGA becomes

$$\frac{M(2\tau)}{M(0)} = e^{-\beta^2}I_0(\beta^2),$$

where I_0 is the zeroth-order modified Bessel function of the

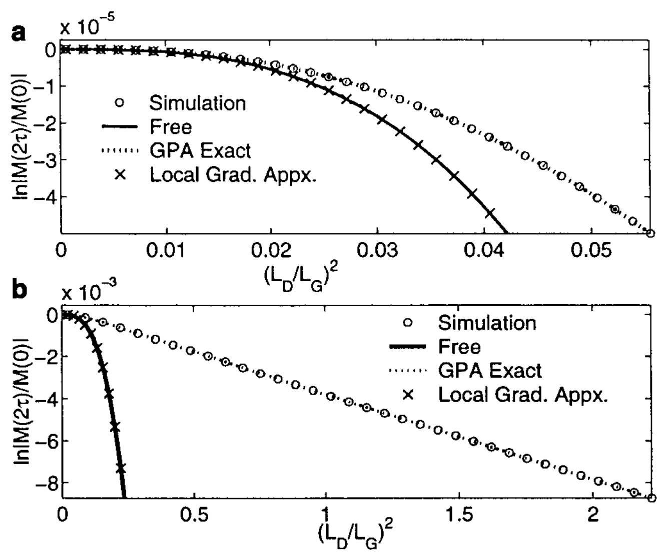

FIG. 9. The local gradient approximation (LGA) for the cosine field (marked by $\times$) vs the simulation data (open circles) and the GPA limits for the first echo in (a) short-time and (b) motionally averaged regimes. Note that due to the vanishing of the first-order short-time correction for this field, the LGA does not even outperform the free-diffusion result while failing, as for the parabolic field, for long times.

TABLE 1
A Compilation of Main Results

$\ln\left(\frac{M(2n\tau)}{M(0)}\right)$	Short time	MAv	Localization	Bounded
Linear	$-\frac{2}{3}(L_D/L_G)^6(n + C(n)(L_D/L_S))$	$\propto L_S^4$	$\propto g^{2/3}$	No
Parabolic	$-\frac{2}{3}(L_D/L_G)^6(n + 1.5\ C(n)(L_D/L_S))$	$\propto L_S^6$	$\propto g_2^{1/2}$	No
Cosine	$-\frac{2}{3}(L_D/L_G)^6(n + \mathbf{0}(L_D/L_S))$	$\propto L_S^2$	$\propto\sqrt{B_0/L_S}$	Yes
LGA	Works	Fails	Fails	
Relevant avg.	$\overline{(\nabla B_z)^2}$	$\overline{(\int dxB_z)^2}$		

first kind, and β is defined as before. In Fig. 8 we compare our simulations in the short-time regime (Fig. 8a) and motionally averaged (Fig. 8b) regime with the LGA prediction.

Apparently, for short times, the LGA works quite well, better than the leading order short-time CPMG result. For long times, however, in the motionally averaged regime, the LGA formula fails dramatically. For the cosine case (see Fig. 9), the LGA does not even work better than Eq. [5], which can be attributed to the vanishing of the first correction in L_D/L_S for the cosine field. Thus it seems that the LGA merely improves upon the short-time result to roughly first order in L_D/L_S and is clearly not applicable at long times.

7. CONCLUSION

Extending previous work on constant gradients, we have investigated the three main regimes of decay of magnetization in a CPMG pulse sequence, the short-time, the motionally averaged, and the localization, for a parabolic and a cosine field. The cosine field is of particular interest because it is a bounded field and thus can be thought of as a crude model of microscopic field inhomogeneities originating near pore boundaries due to strong susceptibility differences near the surface and resulting in bounded fields. We found that the GPA is applicable to both the short-time and the motionally averaged regimes for both fields, while breaking down in the localization regime, where in both cases the long-time decay exponent scales as $\sqrt{B}$.

In the short-time and motionally averaged regimes for both fields we found good agreement between our numerical simulations and the predictions derived from the general GPA solution of Eq. [4]. In the motionally averaged regime, we examined the scaling of the decay exponent with the sample dimensions and found for the cosine field, $\sim L_S^2$, and for the parabolic field, $\sim L_S^6$, compared to the uniform gradient case where $\sim L_S^4$. The weaker pore-size dependence of the cosine field relative to either the linear or the parabolic fields is a general feature of bounded vs unbounded magnetic fields. This result also agrees with the heuristic argument (*2, 24, 28*) that the decay rate is proportional to the spread of the magnetic field squared, $(\Delta B)^2$, times the correlation time. Now for the constant gradient, $(\Delta B)^2 \propto L_S^2$, and for the parabolic field, $(\Delta B)^2 \propto L_S^4$, but for a bounded field $(\Delta B)^2$ is independent of L_S. If we take the correlation time in the MAv regime to be L_S^2/D_0, we obtain the decay rates as L_S^4, L_S^6, and L_S^2 for the constant gradient, parabolic and the bounded field, respectively.

In the motionally averaged regime we also verified that the soft boundary condition, as implemented by Le Doussal and Sen (*24*), does not adequately model a realistic wall, predicting an excessively rapid rate of signal decay.

Of greatest practical interest experimentally are the short-time and motionally averaged regimes where our numerical simulations suggest that the evolution of the signal is largely determined for *all* time solely by the two "moments" of the magnetic field, $\overline{(\nabla B_z)^2}$ and $\overline{(\int dxB_z)^2}$, and not by the details of its local structure.

Finally, for the two fields under consideration, we tested the applicability of the local gradient approximation, a procedure which time-evolves the magnetization according to some local effective gradient, and found that it holds only in the short-time limit and is invalid for longer times.

For easy reference we highlight the major points of our analysis in Table 1.

ACKNOWLEDGMENTS

We are grateful to Scott Axelrod and Axel Andre, whose work on the constant gradient case laid the foundation for this paper. Work at Harvard was supported in part by NSF Grant DMR 94-16910.

REFERENCES

1. P. N. Sen, A. Andre, and S. Axelrod, *J. Chem. Phys.* **111,** 6548 (1999).
2. J. C. Tarczon and W. P. Halperin, *Phys. Rev. B* **32,** 2798 (1985).
3. E. L. Hahn, *Phys. Rev.* **80,** 580 (1950).
4. H. Y. Carr and E. M. Purcell, *Phys. Rev.* **94,** 630 (1954).
5. S. Meiboom and D. Gill, *Rev. Sci. Instrum.* **29,** 688 (1958).
6. T. M. deSwiet and P. N. Sen, *J. Chem. Phys.* **100,** 5597 (1994).
7. C. H. Neumann, *J. Chem. Phys.* **60,** 4508 (1974).
8. P. W. Kuchel, A. J. Lennon, and C. Durrant, *J. Magn. Reson. B* **112,** 1 (1996).
9. B. Robertson, *Phys. Rev.* **151,** 273 (1966).
10. D. J. Bergmann and K.-J. Dunn, *Phys. Rev. E.* **52,** 6516 (1995).
11. R. J. S. Brown and P. Fantazzini, *Phys. Rev. B* **47,** 14823 (1993).

12. P. T. Callaghan, "Principles of NMR Microscopy," Oxford Univ. Press, Oxford, 1991.

13. See numerous references to STRAFI in P. J. McDonald, *Prog. NMR Spectrosc.* **30,** 69 (1997); A. D. Bain and E. W. Randall, *J. Magn. Reson. A* **123,** 49 (1996).

14. R. L. Kleinberg, A. Sezginer, D. D. Griffin, and M. Fukuhara, *J. Magn. Reson.* **97,** 466 (1992).

15. M. N. Miller, Z. Paltiel, M. E. Gillen, J. Granot, and J. C. Bouton, *Soc. Petrol. Eng.* **20,** 365 (1990).

16. P. N. Sen and S. Axelrod, *J. Appl. Phys.* **86,** 8 (1999).

17. S. Majumdar and J. C. Gore, *J. Magn. Reson.* **78,** 41 (1988).

18. R. M. Weisskoff, C. S. Zuo, J. L. Boxerman, and B. R. Rosen, *Magn. Reson. Med.* **31,** 601 (1994).

19. S. D. Stoller, W. Happer, and F. J. Dyson, *Phys. Rev. A* **44,** 7459 (1991).

20. Y. Q. Song, S. Ryu, and P. N. Sen, *Nature* **406,** 178 (2000).

21. H. C. Torrey, *Phys. Rev.* **104,** 563 (1956).

22. M. D. Hürlimann, K. G. Helmer, T. M. de Swiet, P. N. Sen, and C. H. Sotak, *J. Magn. Reson. A* **113,** 260 (1995).

23. S. Axelrod and P. N. Sen, preprint (1999).

24. P. Le Doussal and P. N. Sen, *Phys. Rev. B* **46,** 3465 (1992).

25. M. Abramowitz and I. A. Stegun, "Handbook of Mathematical Functions," Dover, New York, 1965.

26. M. D. Hürlimann, *J. Magn. Reson.* **131,** 232 (1998).

27. P. Bendel, *J. Magn. Reson.* **86,** 509 (1990).

28. R. C. Wayne and R. M. Cotts, *Phys. Rev.* **151,** 264 (1966).